

AD-A038 032

NAVAL RESEARCH LAB WASHINGTON D C

F/6 20/6

A COMPARISON OF MEASURED 3.8 MICRON SCATTERING FROM NATURALLY 0--ETC(U)

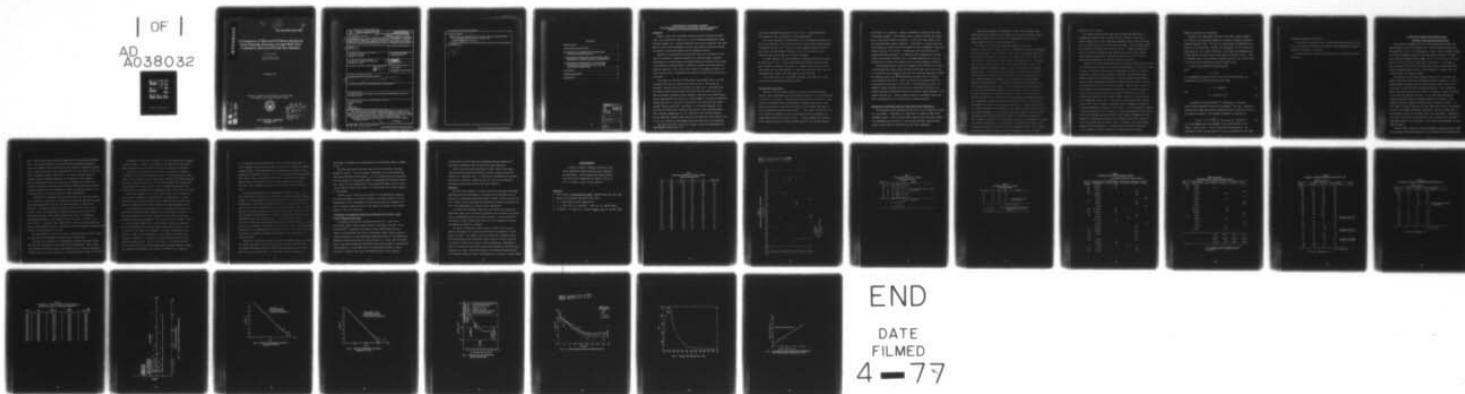
FEB 77 P M LIVINGSTON

UNCLASSIFIED

NRL-MR-3450

NL

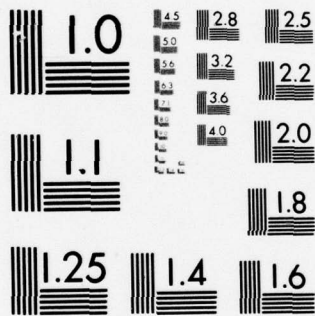
| OF |
AD
A038032



END

DATE
FILMED

4-77



MICROCOPY RESOLUTION TEST CHART
NATIONAL BUREAU OF STANDARDS-1963-A

AD A 038032

12
NRL Memorandum Report 3450

A Comparison of Measured 3.8 Micron Scattering From Naturally Occurring Aerosols With That Predicted by Measured Particle Size Statistics

P. M. LIVINGSTON

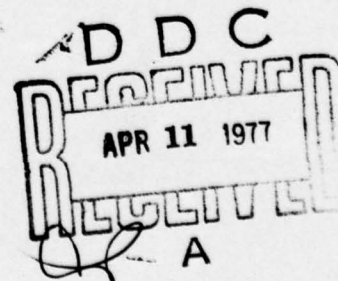
*Optical Radiation Branch
Optical Sciences Division*

February 1977

This work was sponsored by the High Energy Laser Project Office
PM-22/PMS-405 of the Naval Sea Systems Command.



NAVAL RESEARCH LABORATORY
Washington, D.C.



AD No. _____
DDC FILE COPY

SECURITY CLASSIFICATION OF THIS PAGE (When Data Entered)

REPORT DOCUMENTATION PAGE		READ INSTRUCTIONS BEFORE COMPLETING FORM
1. REPORT NUMBER NRL Memorandum Report 3450	2. GOVT ACCESSION NO. (14)	3. RECIPIENT'S CATALOG NUMBER NRL-MR-3450
4. TITLE (and Subtitle) A COMPARISON OF MEASURED 3.8 MICRON SCATTERING FROM NATURALLY OCCURRING AEROSOLS WITH THAT PREDICTED BY MEASURED PARTICLE SIZE STATISTICS.		5. TYPE OF REPORT & PERIOD COVERED Interim report on a continuing NRL problem, July 75-October 75.
7. AUTHOR(s) P.M./Livingston		6. PERFORMING ORG. REPORT NUMBER
9. PERFORMING ORGANIZATION NAME AND ADDRESS Naval Research Laboratory Washington, D.C. 20375		8. CONTRACT OR GRANT NUMBER(s)
11. CONTROLLING OFFICE NAME AND ADDRESS Naval Sea Systems Command (PM-22/PMS-405) Washington, D.C. 20362		10. PROGRAM ELEMENT, PROJECT, TASK AREA & WORK UNIT NUMBERS NRL Problem R05-31A
14. MONITORING AGENCY NAME & ADDRESS (if different from Controlling Office) (12) 34P		12. REPORT DATE February 1977
		13. NUMBER OF PAGES 33
		15. SECURITY CLASS. (of this report) UNCLASSIFIED
		15a. DECLASSIFICATION/DOWNGRADING SCHEDULE
16. DISTRIBUTION STATEMENT (of this Report) Approved for public release; distribution unlimited.		
17. DISTRIBUTION STATEMENT (of the abstract entered in Block 20, if different from Report) (9) Interim rept. Jul - Oct 75,		
18. SUPPLEMENTARY NOTES This work was sponsored by the High Energy Laser Project Office PM-22/PMS-405 of the Naval Sea Systems Command.		
19. KEY WORDS (Continue on reverse side if necessary and identify by block number) Atmospheric scattering Aerosol Laser Nephelometry Particle spectrometry		
20. ABSTRACT (Continue on reverse side if necessary and identify by block number) Recent field measurements of scattered 3.8 micron laser radiation from naturally occurring aerosols were made during a four-week period in coastal Southern California. Simultaneously, aerosol distribution measurements were made which, in conjunction with MIE scattering theory, gave estimates of the volume scattering coefficient at the various angles. A comparison shows that: (1) (a) Calculated volume scattering coefficients generally decrease more rapidly in angle than measurements indicate; and (2) (Continued on p. ii)		

DD FORM 1 JAN 73 1473

EDITION OF 1 NOV 65 IS OBSOLETE
S/N 0102-014-6601

SECURITY CLASSIFICATION OF THIS PAGE (When Data Entered)

251 950

20. Abstract (Continued) *e A pic*

(b) On the average, the calculation gives factor of 2 larger volume backscattering coefficients than measured, but underpredicts forward scattering by 33%.

A second, unrelated observation of interest:

Volume scattering coefficients in the visible showed 65% correlation with 3.8 micron backscatter (177) coefficients. *deg*

CONTENTS

INTRODUCTION	1
THE PARTICLE SIZING SYSTEM	2
ESTIMATION OF SCATTERING COEFFICIENT FROM PARTICLE SIZE DISTRIBUTION	3
A COMPARISON OF MEASURED AND ESTIMATED ANGLE — DEPENDENT VOLUME SCATTERING COEFFICIENTS	8
A COMPARISON OF EXPERIMENTAL BACKSCATTER- COEFFICIENTS WITH VISIBLE (.65 μ m) VOLUME SCATTERING COEFFICIENTS	12
CONCLUSION	13
ACKNOWLEDGEMENTS	14
REFERENCES	14

ACCESSION slip	
BY	White Section <input checked="" type="checkbox"/>
DDO	Defl Section <input type="checkbox"/>
UNANNOUNCED	<input type="checkbox"/>
JUSTIFICATION	
BY	
DISTRIBUTION/AVAILABILITY CODES	
Dist.	AVAIL. CODE/SPECIAL
A	

A COMPARISON OF MEASURED 3.8 MICRON
SCATTERING FROM NATURALLY OCCURRING AEROSOLS WITH THAT
PREDICTED BY MEASURED PARTICLE SIZE STATISTICS

Introduction

During a recent field experiment conducted along the Southern California coast, four laboratories cooperated in a joint scattering measurements program. TRW Space Systems, Inc., Lockheed Laboratory, and Avionics Laboratory (Air Force) made the actual light measurements, and the Naval Research Laboratory provided the particle counting measurements and the subsequent analysis.

Reasons for the measurement program were varied, but the purpose of this paper is to develop a comparison between actual measured volume scattering coefficients (at various angles) and similar quantities calculated from particle size statistics, an assumed index of refraction, and MIE scattering theory for spherical particles. Data, such as this, taken in the middle IR region, are rare, and rarer still is comparison with predictions derived from particle size statistics.

The program was carried out during August and September 1975 at the TRW Capistrano Test Site, six hundred feet above sea level. The weather was reasonably constant during the evolution of a typical day. Each morning the sea-induced coastal fog would burn off by 1000 hours and return after dark when the offshore continental breeze subsided. Individual days showed meteorological range varying from infinity to a few kilometers, and relative humidities varying from 30% (~ 8 torr H_2O) to over 80% (14 torr H_2O) with the average humidity centered around 50%. (See Table 1.) On several occasions, a hot, dry wind (the "Santa Anna" condition) blew from the upper California desert-land, elevating temperatures to $\sim 30^\circ$ (with 50% or less relative humidity). During these days, numerous brush fires were also observed in the vicinity, but on only one occasion were measurements made with smoke haze in the beam path.

The laser source was a multiline DF chemical laser with approximately 22

Note: Manuscript submitted January 21, 1977.

lines whose wavelengths ranged from $3.6\mu\text{m}$ to $4.0\mu\text{m}$. A focused 76cm beam was transmitted over a 1.5km path to a collecting station.

The various laboratory's instrumentation will be described elsewhere, but here it is sufficient to note that each group's field of view appeared adequate to intercept the full beam. Moreover, certain alignment checks were made to insure that the beam remained centered in the FOV of each device as the instrument angle with respect to the beam was changed.

By common agreement each group reported its volume scattering coefficient in units of $\text{km}^{-1} \text{ster}^{-1}$. Overall calibration was determined from the instrument sensitivity calibration (traceable to a commonly used black-body source), laser power, FOV, and path geometry. In some cases extinction losses from the intercepted beam volume to the instrument were also estimated.

Since these issues will be addressed elsewhere, this paper will concentrate on the intercomparison described earlier.

The Particle Sizing System

The device used for aerosol particle counting was Particle Measuring Systems' Active Scattering Aerosol Spectrometer (referred to as the "Knollenberg" system after its designer). The basic operating principle is similar to other counters---intercepted light is scattered into collecting optics and, by calibration with known size particles, the height of the scattered light pulse is used to determine the particle cross section. In most cases the light source is an incoherent lamp brought to focus in the sample volume and blocked by an opaque disk just beyond the point of focus. A large condenser lens (centered on the field stop) collects scattered light produced by the particle passage

and focuses it on a detector. Unless 2μ steradians is covered by the field-lens-detector geometry, the instrument gives an apparent particle size dependent on the particle index of refraction. In the usual case, however, only the forward scattered light is measured. In addition to a serious refractive index dependence, signal-to-noise considerations limit measurement of particles smaller than about $0.1\mu\text{m}$ radius. An additional practical difficulty with standard instruments intrudes: the particles must be brought into the focal volume, necessitating "plumbing" with an attendant modification of the size distribution due both to wall adherence and to relative humidity variations.

The Knollenberg device partially circumvents these difficulties by using a forced aspiration system to pass the particles through a HeNe laser cavity. The airflow and cavity optics are such that the cavity beam essentially defines the sampling volume, thus eliminating small bore piping and the attendant size distribution distortion. Light is collected and scattered beyond one cavity mirror in the range 4° to 22° (170° - 150° backscatter) giving a considerably larger collection solid angle than conventional instruments and thereby achieving a significant reduction in refractive index dependence of the apparent particle size. Lastly, signal-to-noise is considerably enhanced by laser flux densities up to 16 times that for incoherent sources.

Estimation of Scattering Coefficient From Particle Size Distribution

The DF chemical laser beam was directed over the 1.5 km range for periods of a few seconds. (These "shots" are identified by a number VLI-XXX in the subsequent tables.) During an eight minute interval about each shot, aerosol size information was collected at a site located 100 meter perpendicularly distant from the beam and 500 meters from the laser transmitter.

A series of experiments had suggested the eight minute averaging time. Long intervals gave "skewed" results because the aerosol distribution changed appreciably, while shorter intervals were unsatisfactory because of the reduced sample statistics of the larger particles.

The range of the Knollenberg instrument extended from $0.10\mu\text{m}$ radius to $5.0\mu\text{m}$ radius. Figure 1 shows the arrangement for the four overlapping particle size ranges. Pulses from the counter head are commutated between the four ranges in a fraction of a second. Pulse height gates, 16 per range, size the "particles" and accumulate counts during the commutator dwell. The results are recorded on digital magnetic tape at one second intervals. Later, intermediate processing averages the number of counts in each "bin" for an eight-minute period. At this stage, numerous numerical experiments were performed with the data in an effort to curve-fit the data (on log-log paper) and to do the subsequent numerical integration over a particle size range extending beyond the instrument range. The idea was to estimate the contributions of a few large particles which, because of their high forward scattering efficiency at $3.8\mu\text{m}$, can significantly contribute to the volume scattering coefficient. To date, the approach has yielded inconclusive results. The uncertainties primarily resulted from irregularities in the size spectrum beyond $2.0\mu\text{m}$, which were inadequately represented by second or third order fits. The best line of investigation for fitted data integration appears to be a weighted second order fit, where the weights are proportioned to the number of counts in each size bin. An alternate approach, the one pursued in this work, eschews the curve-fit and approximates the volume scattering coefficient as a "histogram integration". Such a result is clearly a lower bound (since the range of the counter is limited) but, within the resolution of the instrument, it reproduces the "bumps" in the large particle end of the range (which have a significant effect on the forward scattering and which may represent quasi-mono-disperse sea salts or pollen

particles at $1.0 \sim 2.0 \mu\text{m}$.)

The final processing of the eight minute average data consisted of combining the particle counts in each of the four ranges to form 720 elementary "quantum bins" (each $.005 \mu\text{m}$ wide) extending from the first bin threshold in the first range to the last in the last range. For each range, quantum bins outside of the range were filled with zeroes. A composite quantum bin range was obtained by averaging like quantum cells across the four ranges. These quantum cells were then collapsed by a factor of 12 to form 60 equispaced bins approximating the original instrument resolution.

Figures 2 and 3 show logarithmic plots of the relative number density versus the relative particle radius for two particular experiments, VL1-168 and VL1-182. As shown in the next section, these two experiments were used to illustrate a comparison of measured angle scattering coefficients and predictions based upon the particle size distribution data. The dots represent "experimental" particle density measurements processed as described above, whereas the solid lines give the best curve-fit to the data points. There is about a factor of three difference in the scattering; the latter shot, VL1-182, being made on a clear, hot, relatively dry day. Yet the shape of the two curves is quite similar, particularly in the vicinity of "bump" at about 1.8 ($1.0 \mu\text{m}$ diameter) on the logarithmic radius scale. Such curves have been seen before; the magnitude of the "bump" increases or decreases (and even disappears altogether in some measurements) but appears to be real data. Current speculation suggests a bimodal distribution in the vicinity of a marine environment with small continental haze particles (giving the initial smooth power-law dependence) superimposed on a characteristic marine haze of larger particle sizes (perhaps of sea salt plus water and sea surface ejecta). Evidence of this type strongly suggests that the assumption of a uniform index of refraction (for water, $n = 1.363 + 0.0039i$ at $3.802 \mu\text{m}$) chosen for all particle sizes is invalid.

However, no better data is available.

Incidentally, the appreciable deviation of the "bump" shown in Figure 2 and 3 was one of the principal reasons for choosing a histogram integration technique mentioned above. The curve fit clearly misses an appreciable contribution to the scattering. Further, the "graininess" of the two plots for large values of r is a counter limitation. Even though the averaging period is eight minutes, the dwell time on each range is one fourth of that. There is, therefore, both a count-statistics variation and poor size resolution due to a bin size choice required to accumulate enough counts.

A table of scattering efficiencies $Q_{sc}(x, \theta)$

where

$$x = 2\pi r/\lambda \quad (1)$$

is the dimensionless particle size, and θ is the scattering angle, was calculated for the 10,000 (x, θ) pairs in the range

$$x \quad [.1 \text{ } (.0295) 6.0] \quad (2)$$

and

$$\theta \quad [2.0^\circ (3.5^\circ) 177^\circ] \quad (3)$$

An algorithm, based upon Kerker's⁽¹⁾ formulation of the Bessel-Riccati Series developed by Hancock and Livingston⁽²⁾ was used. Consistency comparison with RAND tables show the double precision calculation is valid to 4-5 significant figures. The histogram integration is thus given by

$$\beta_{sc}(\theta) = \pi k^{-3} 10^{-3} \sum_{j=1}^{60} x_j^2 n(x_j) Q_{sc}(x_j, \theta) \text{ [km}^{-1} \text{ster}^{-1}]; \quad (4)$$

x_j^2 is the dimensionless area parameter; $n(x_j)$ [particles/cm³] is the number of counts in bin j ; and Q_{sc} is the scattering efficiency. The wavenumber k ($=2\pi/\lambda$) and the factor 10^{-3} scale the dimensions of the volume

scattering coefficient to $\text{km}^{-1}\text{ster}^{-1}$.

It was found by measurement that the laser beam was unpolarized, so that the Q_{sc} is actually the average of the parallel and perpendicular component Q relative to the plane of scattering.

In the next section calculations based upon Eq. 4 are compared with the field data.

A Comparison of Measured and Estimated Angle-
dependent Volume Scattering Coefficients

Table 2 gives a schematic over-view of the scattering data taken from the 8th through the 19th of September 1975. Thirteen scattering angles were investigated for a total of 61 measurements. Figure 4 shows a schematic giving the relative placement and range of each experimenter's results. As shown later, Avionics Laboratory results appear low (by a factor of four or so) relative to the other groups for reasons still under study. At this time, it does not appear to be the result of beam-receiver field-of-view misalignment. (That was checked during the course of the experiment.) Further, the ratio to other groups' data appears constant.

For the particle distribution measured during each of the shots, the angular scattering function was calculated according to Equation 4. Each resulting angular scattering function estimate was then summed over the full solid angle to yield the total scattering coefficient. Then a normalized angular scattering function was calculated by dividing the angular scattering by the total scattering for each shot. All of these normalized angular scattering functions were then averaged together at each angle to give a composite normalized angular scattering, which is graphed in Figure 5. In that figure, the chain dotted and the chain dashed lines show the area bounded by one and two standard deviations, respectively, from the average value of the function at each of the 50 angles used in the calculations. Additionally, each run's calculated total scattering was used to normalize the scattering measurements made by the three groups. Their normalized measurements are also shown in Figure 5.

Beyond a direct comparison, two semi-independent quantities (derived from the calculated scattering coefficient) can be inferred from the multiple angle

data. These are the relative shape and magnitude of the scattering coefficient curve. The relative shape can be inferred by taking forward-to-backscatter ratios and comparing them to similar ratios from forward to backscatter measurements. Tables 3 and 4 show ratio comparisons for 5° to 177° and 19° to 177° forward-to-backscatter angles, respectively. The choice of angles (which was somewhat arbitrary) depended primarily on the quantity of data available. Since it became clear during the course of the experiment that possibly two different populations of particles were involved (forward scattering from water droplets and backscatter from condensation nuclei) the ratios may prove to be a sensitive test of the uniform refractive index approximation.

A comparison of scattering based upon the particle size data with measurement is essentially statistical in nature since the particle sampling instrument was located some distance away from the sampled region(s) of the IR beam. Therefore, a significant indicator in Tables 3 and 4 is the "ratio of ratios" average. This is the experimental forward/backscatter ratio divided by the theoretical estimate (shown as R_E/R_T) averaged over the set of experiments. Were agreement perfect, on the average, the ratio is unity. In Table 3, the ratio is 1.03. To interpret this "sample mean" as drawn an infinite population mean, we apply sample statistics. The result is that the hypothesis "population mean is unity" is valid with only a 5% risk.

The same situation is not true in Table 4, where the ratio of ratios average is only 0.16 and the hypothesis "population mean is unity" fails.

Therefore, on the average, the experimental scattering curve might appear shallower than the prediction based upon particle distribution. Such a result could represent the upper and lower range limitation of the counting instrument (5.0 μ m) as well as an effect produced by a non-uniform particle index of refraction.

An extension of the "ratio of ratios" to all other combinations of angles, is shown in Table 5. Since the data based is very limited for some angles, a rigorous application of small sample statistics is probably not warranted.

Instead, the chief utility of the table is to establish the internal consistency of the various experimental groups. As alluded to earlier, there appears to be a problem with the Avionics data as shown by the largest deviation from unity of the average shown in the "Avionics-Lockheed" and "Avionics-TRW" forward/backscatter columns. However, only the TRW-TRW forward/backscatter average admits the hypothesis that the population mean is unity with a 10% risk.

Lastly there appears to be a trend in both Tables 5 and 6 in which the ratios tend to approach unity with increasing time (experience). If true, then some of the earlier data showing large variations could be partly interpreted as systematic error which was reduced with increased operator skill.

As shown previously, there appears to be a systematic deviation in the measured and calculated angular dependence of the scattering coefficient. The next major question is how well the magnitude of the predicted scattering coefficient agrees with measurement. The results for 177° are shown in Table 6. The ratio shown suggests that, on the average, calculation based upon particle distribution and an assumed index of refraction for water at $3.8\mu\text{m}$ is a factor of two larger than experiment. The trend from smaller to larger numbers is evident as time progresses, but the scatter in the table also increases. Therefore, it is difficult to judge whether the trend to unity average has become stable. Runs VLI-170, VLI-176, VLI-179 gave unusually large deviations from the average trend and were eliminated from the average. The reasons for this behavior are unclear, but probably can be traced to

in the input particle distribution data. Note that approximately 70% of the measurements and calculations correlate in spite of the different sampling volumes involved. This encouraging feature suggests that the small particle population is reasonably uniform in space. The factor-of-two average disagreement between theory and experiment can probably be reduced by co-locating sample volumes, by obtaining index of refraction measures for the small particles, and by extending the range of the instrument to larger particle sizes.

Forward scattering prediction comparisons are shown in Table 7. Here again data scatter is large, and no trend with increasing experiment number is evident. Less encouraging than the previous result is the low coefficient of determination. Even though the predictions are only 33% low on the average, only 28% of the data and corresponding calculations correlate. There are three possible (and likely) explanations. First, the Knollenberg instrument shows size resolution problems beyond $2.5\mu\text{m}$ radius in which $3.0\mu\text{m}$ particles are not distinguished from those smaller in size. Second, the small number of particles in these size ranges (containing the more efficient forward scatterers) leads to count statistics fluctuations. Last, it may be that the large particle population is very inhomogeneously distributed in space. The latter issue could be resolved by looking for increased correlation in a co-located sampling volume experiment.

Figure 6 is a graph which shows the relative contribution which scattering at a given angle makes to the total scattering. The curve was obtained by multiplying the average normalized angular scattering function by $2\pi \sin\theta$, where θ is the scattering angle. It represents the total scattering at a

given angle, as opposed to the scattering per unit solid angle which is graphed in Fig. 5.

Note that two thirds of the area under the curve lies within the range between 10° and 50° . Since the greatest contribution to the total scattering comes from scattering at these angles, it is to be expected that the scattering from this region will have greater weight in determining the normalized scattering. Hence, both the "necking down" of the standard deviation curves in Figure 5 and the peak in Figure 6 are effects to be associated with the solid geometry of this problem.

Finally, as can be seen from the location of the experimentally measured data points in Figure 5, more data is needed in the range between 10° and 50° . Consideration of the solid geometry involved (particularly as evidenced by the curve in Figure 6) shows that data in this region will provide a more reliable measure of the total scattering.

A Comparison of Experimental Backscatter-Coefficients with Visible ($.65\mu\text{m}$) Volume Scattering Coefficients

One question that has been considered for some time is "What is the relationship between visible range and aerosol scattering in the IR?" Curcio and Knestrick⁽⁴⁾ considered the problem in several papers some years ago. Clearly, if the particles most active in scattering visible light also produce a major contribution to $3.8\mu\text{m}$ backscatter radiation relative to the (inefficient) backscatter contributions from the large particles ($r \sim 1.7\mu\text{m}$), then the visible range or the volume scattering coefficient derived from it ought to correlate with $3.8\mu\text{m}$ backscatter. On the other hand, the scattering efficiency of "small particles" at $3.8\mu\text{m}$ is very low, so the question turns on one of balance

"Do many small particles with poor scattering efficiency dominate the backscatter contribution from the many fewer larger particles?"

Table 8 gives the results and Figure 7 shows a plot of the visible volume scattering coefficient (measured by optical pyrometry) versus the Lockheed 177° backscatter data. A coefficient of determination of 65% shows considerable correlation, suggesting that over half of the backscatter contribution arises from visible-active small particles.

Conclusion

The above study suggests an overall picture of mid-IR light scattering predicted from haze distributions. The shape of the scattering curve reproduces the experimental measurement ratios to within a factor of two or so, with a factor of two overestimate for backscatter coefficient prediction and with a 38% underestimate for forward scatter coefficients.

It appears that instrument range limitations affect both forward and backscatter values of the scattering coefficient with the index-of-refraction question predominantly open for the small particles. Detailed analysis of the refractive index variation with particle size is required for further improvements in predictive capability.

The amount of backscatter "glory" shown in Figure 5 may be used to identify how irregular the scattering particles are according to a recent paper in Science⁵. The authors claim that better fits to angular scatter data from microscopically identified "rough" particles follow by reducing the amount of surface wave present in the MIE calculation. Measurements given in this paper are not precise enough to infer particle population size regularity, but open a fascinating prospect for roughness estimation based upon numerical fitting of surface wave magnitude as a function of Bessel index.

ACKNOWLEDGEMENTS

A number of people at Lockheed, TRW and Air Force Avionic Laboratory kindly provided me with information and good advice. Critical manuscript reading and editing as well as the computation for Figure 6 are due to Dr. K. M. Haught to whom I am most grateful.

References

1. Milton Kerker, The Scattering of Light, Academic Press, New York, 1969.
2. Hancock and Livingston, NRL Report 7808 (1974).
3. W. L. Shackelford, Private Communication.
4. J. A. Curcio and G. L. Knestrick, J. Opt. Soc. Am., 48 686 (1958).
5. P. Chylek, G. W. Grams, R. G. Pinnick, Science, 193, pp. 480-482 (1976).

Table 1
Temperature, Relative and Absolute Humidity
During Experiment Times

DATE	TIME	EXPT NO.	TEMP °C	RH(%)	H ₂ O PRES(TORR)
9/8	1735	VL1-157	17.8 ⁰	86.2	13.2
9/9	1628	-158	18.1	80.3	12.5
9/9	1858	-159	17.1	88.7	13.0
9/10	1309	-160	19.8	69.5	11.9
9/10	1552	-161	20.6	62.8	11.4
9/10	1902	-162	17.1	75.8	11.1
9/11	1318	-163	21.6	58.6	11.3
9/11	1552	-164	20.3	61.1	10.9
9/12	1200	-165	19.6	71.7	12.2
9/12	1420	-166	20.1	72.1	12.8
9/12	1642	-167	18.3	80.1	12.6
9/12	1815	-168	17.2	87.1	12.8
9/15	1259	-169	27.2	45.7	12.4
9/16	1233	-170	32.8	30.3	11.3
9/16	1820	-171	25.2	30.2	8.6
9/17	1133	-172	31.0	31.8	10.7
9/17	1332	-173	29.6	39.5	12.3
9/17	1447	-174	29.9	40.3	12.8
9/17	1650	-175	30.2	37.8	12.2
9/17	1916	-176	26.0	44.2	11.2
9/18	1048	-177	27.2	46.9	12.7
9/18	1404	-179	28.9	36.2	10.3
9/18	1542	-180	27.5	32.1	8.9
9/19	1226	-181	25.7	43.3	10.7
9/19	1523	-182	25.1	53.4	12.8
9/19	1807	-183	22.7	62.6	13.0

BEST AVAILABLE COPY

Table 2
Scattering Angle Measurement Distribution

EXPT NO.	THEORY (NRL)	SCATTERING ANGLE													
		5° TRW	12.8° AV	15.0° TRW	17° TRW	19.0° TRW	28.9° AV	47.4° TRW	75° TRW	101.7° AV	161° TRW	163° TRW	175° TRW	177° (L)	
VL1-157	NC			X										X	
-158	X		X											X	
-159	X						X							X	
-160	X			X										X	
-161	X													X	
-162	X													X	
-163	X					X					X			X	
-164	X					X					X			X	
-165	X													X	
-166	X								X					X	
-167	X								X					X	
-168	X								X					X	
-169	X								X					X	
-170	X								X					X	
-171	X													X	
-172	X													X	
-173	X													X	
-174	X													X	
-175	X													X	
-176	X													X	
-177	X													X	
-178	X													X	
-179	X													X	
-180	X													X	
-181	NC													X	
-182	X													X	
-183	X													X	
-184	X													X	
-185	X													X	
-186	X													X	
-187	X													X	
-188	X													X	
-189	X													X	
-190	X													X	
-191	X													X	
-192	X													X	
-193	X													X	
-194	X													X	
-195	X													X	
-196	X													X	
-197	X													X	
-198	X													X	
-199	X													X	
-200	X													X	
-201	X													X	
-202	X													X	
-203	X													X	
-204	X													X	
-205	X													X	
-206	X													X	
-207	X													X	
-208	X													X	
-209	X													X	
-210	X													X	
-211	X													X	
-212	X													X	
-213	X													X	
-214	X													X	
-215	X													X	
-216	X													X	
-217	X													X	
-218	X													X	
-219	X													X	
-220	X													X	
-221	X													X	
-222	X													X	
-223	X													X	
-224	X													X	
-225	X													X	
-226	X													X	
-227	X													X	
-228	X													X	
-229	X													X	
-230	X													X	
-231	X													X	
-232	X													X	
-233	X													X	
-234	X													X	
-235	X													X	
-236	X													X	
-237	X													X	
-238	X													X	
-239	X													X	
-240	X													X	
-241	X													X	
-242	X													X	
-243	X													X	
-244	X													X	
-245	X													X	
-246	X													X	
-247	X													X	
-248	X													X	
-249	X													X	
-250	X													X	
-251	X													X	
-252	X													X	
-253	X													X	
-254	X													X	
-255	X													X	
-256	X													X	
-257	X													X	
-258	X													X	
-259	X													X	
-260	X													X	
-261	X													X	
-262	X													X	
-263	X													X	
-264	X													X	
-265	X													X	
-266	X													X	
-267	X													X	
-268	X													X	
-269	X													X	
-270	X													X	
-271	X													X	
-272	X													X	
-273	X													X	
-274	X													X	
-275	X													X	
-276	X													X	
-277	X													X	
-278	X													X	
-279	X													X	
-280	X													X	
-281	X													X	
-282	X													X	
-283	X													X	
-284	X													X	
-285	X													X	
-286	X													X	
-287	X													X	
-288	X													X	
-289	X													X	
-290	X													X	
-291	X													X	
-292	X													X	
-293	X													X	
-294	X													X	
-295	X													X	
-296	X													X	
-297	X													X	
-298	X													X	
-299	X													X	
-300	X													X	
-301	X													X	
-302	X													X	
-303	X													X	
-304	X													X	
-305	X													X	
-306	X													X	
-307	X													X	
-308	X													X	
-309	X													X	
-310	X													X	
-311	X													X	
-312	X													X	
-313	X													X	
-314	X													X	
-315	X													X	
-316	X													X	
-317	X													X	
-318	X													X	
-319	X													X	
-320	X													X	
-321	X													X	
-322	X													X	
-323	X													X	
-324	X													X	
-325	X													X	
-326	X													X	
-327	X													X	
-328	X													X	
-329	X													X	
-330	X													X	

L. LOCKHEED CORP.
AV ELECTRONICS LAB.
TRW, INC.
NRL NAVAL RESEARCH LABORATORY
NC NOT COMPLETE

Table 3
A Comparison of 5° to 177° Forward
to Backscatter Ratios

SHOT NO VL 1	R _E	R _T	R _E /R _T	COMMENTS
-174	195.4	168.6	1.16	Theory calculation suspect: eliminated from average.
-175	108.3	101.6	1.06	
-176	527.3	33.5	15.7	
-177	182.3	163.8	1.1	
-178	41.6	107.2	.387	
-179	84.7	204.7	.42	
-182	172.9	84.4	2.05	

1.03 AV ± .60(STD DEV)

$$R_E = \rho_E(5^\circ) / \rho_E(177^\circ)$$

$$R_T = \rho_T(5^\circ) / \rho_T(177^\circ)$$

Table 4
A Comparison of 19° to 177° Forward
to Backscatter Ratios

SHOT No. VLL	R _E	R _T	R _E /R _T	COMMENTS
-163	17.3	66.9	.259	
-164	10.3	80.7	.128	
-176	481.8	26.8	.056	Theory calculation suspect: eliminate from A'vg.
-182	24.1	67.7	.356	
<hr/>				
.161 AV ± .15 (STD DEV)				
$R_T = R_F(19^\circ)/R_F(177^\circ)$		Conclusion: Average forward-to-backscatter ratio less than calculated from particle distribution.		
$R_T = R_T(19^\circ)/R_T(177^\circ)$				

Table 5
A Comparison of the Various Laboratory's Results

$$A = R_E(\text{Angle}(1)/\text{Angle}(2))/R_T(\text{Angle}(1)/\text{Angle}(2))$$

— A —

Shot No. 1	Angle(1)/Angle (2)	Avionics/Lockheed	Avionics/TRW	TRW/Lockheed	TRW/TRW
VL1-158	12.8/177°	.257			
-159	28.9/177°	.109			
-160	16°/177°			.243	
-163	19°/177°			.260	
	161°/177°			.204	
	19/161°				.993
-164	19/177°			.127	
	161/177°			.203	
	19/161°				.625
-166	101.7/177°	.185			
-167	101.7/177°	.550			
-168	16°/177°			.134	
	101.7/163°		.951		
	101.7/177°	.551			
	16/163°				.231
	163°/177°			1.05	
-170	167°/177°			.699	
-171	175°/177°			2.13	
-174	5°/177°			1.16	
-175				1.07	
-177	5°/177°			1.11	
	47.4/177°	.585			
	5/47.4°		1.9		
-178	5°/177°			.388	
-179	5°/177°			.420	

Table 5 (Continued)
A Comparison of the Various Laboratory's Results

Shot No. 1	Angle(1)/Angle(2)	Avionics/Lockheed	Avionics/TRW	TRW/Lockheed	TRW/TRW
-180	5°/19°				.71
-182	5°/177°	1.37			
	5°/75°				.698
	5°/19.5°		3.88		
	5°/17°				.674
	17°/19.5°		5.75		
	17/75°				1.036
	17°/177°				2.05
	19.5°/75°		.18		
	19.5°/177°		.356		
	75°/177°				1.977
-183	5°/75°				4.15
	5°/19.5°		3.18		
	5°/17°				.554
	17/75°				7.48(?)
	17/19.5°		5.74		
	19.5°/75°		1.30		
		.515 AV	2.58 AV	.657 AV	1.24 AV
		± .46	± 2.17	± .584	± 1.19
		STD DEV	STD DEV	STD DEV	STD DEV
		VAR=.901	VAR=1.2	VAR=.89	VAR=.902

Avionics/Lockheed, Avionics/TRW average ratios show greatest deviation from unity suggesting internal inconsistency.

Table 6
Comparison of Measured and Predicted Backscatter at 177°

$\beta(\theta) [\text{km}^{-1}\text{ster}^{-1}] \times 10^4$				
SHOT NO.	177° Exp.	177° Theo.	Ratio: Exp/Theory	Comments
VL1-158	3.3	8.9	.371	
-159	4.03	7.38	.546	
-160	2.11	7.07	.298	
-161	2.09	8.94	.233	
-162	1.95	3.60	.542	
-163	2.48	5.68	.437	
-164	3.02	9.30	.325	
-166	4.72	11.4	.414	
-167	3.42	14.8	.231	
-168	3.44	16.2	.212	
-169	5.72	30.9	.185	
-170	4.16	44.1	.094	Calculation questionable: eliminate from average.
-171	1.83	6.3	.290	
-174	1.74	3.44	.505	
-175	1.20	.702	1.71	
-176	1.10	.282	3.90	Calculation questionable: eliminate from average.
-177	3.18	9.46	.336	
-178	1.25	1.38	.905	
-179	2.95	1.075	2.74	Calculation questionable: eliminate from average.
-181	2.29	2.01	1.14	
-182	2.95	5.39	.547	
			.513	Average slope

Coefficient of Determination: 70%

Table 7
Comparison of Measured and Calculated Forward Scatter at 5°

$\beta [\text{km}^{-1} \text{ster}^{-1}] \times 10^2$			
SHOT NO. 1	5° Exp.	5° Theo.	Ratio: Exp/Theory
VLI-172	3.8	2.7	1.41
-173	3.0	2.34	1.28
-174	3.4	5.8	.58
-175	1.3	.71	1.83
-176	5.5	.0089	651.6 Calculation suspect: eliminate from average.
-177	5.6	15.5	.374
-178	5.2	1.48	3.51
-179	2.5	2.2	1.13
-180	2.3	4.1	.56
-181	4.9	3.1	1.58
-182	6.2	8.2	.756
-183	8.7	5.2	1.67
1.33 Average ratio			

Coefficient of Determination: 28%

Table 8
A Comparison of "Visible" Volume Scattering Coefficients
(Divided by 4π) and 177° Backscatter Coefficients

DATE	TIME	km^{-1} $\sigma_{3.8\mu}(177^\circ)$	km^{-1} $\sigma_{.65\mu}/4\pi$	RATIO $\frac{\sigma_{.65\mu}}{\sigma_{3.8\mu}}$
9/10	1309	2.11-4	8.75-3	41.46
9/10	1552	2.09-4	9.55-3	45.69
9/10	1902	1.95-4	9.55-3	48.97
9/11	1318	2.48-4	1.23-2	49.59
9/12	1420	4.72-4	2.39-2	50.64
9/15	1259	5.72-4	4.38-2	76.57
9/16	1233	4.16-4	8.75-3	20.99
9/16	1820	1.83-4	7.16-3	39.12
9/17	1447	1.74-4	5.88-3	33.87
9/17	1650	1.2-4	5.65-3	47.08
9/17	1916	1.1-4	3.18-3	28.91
9/18	1048	3.18-4	7.08-3	22.26
9/18	1247	1.25-4	4.13-3	33.04
9/18	1404	2.95-4	3.82-3	12.95
9/19	1523	2.95-4	7.88-3	26.71

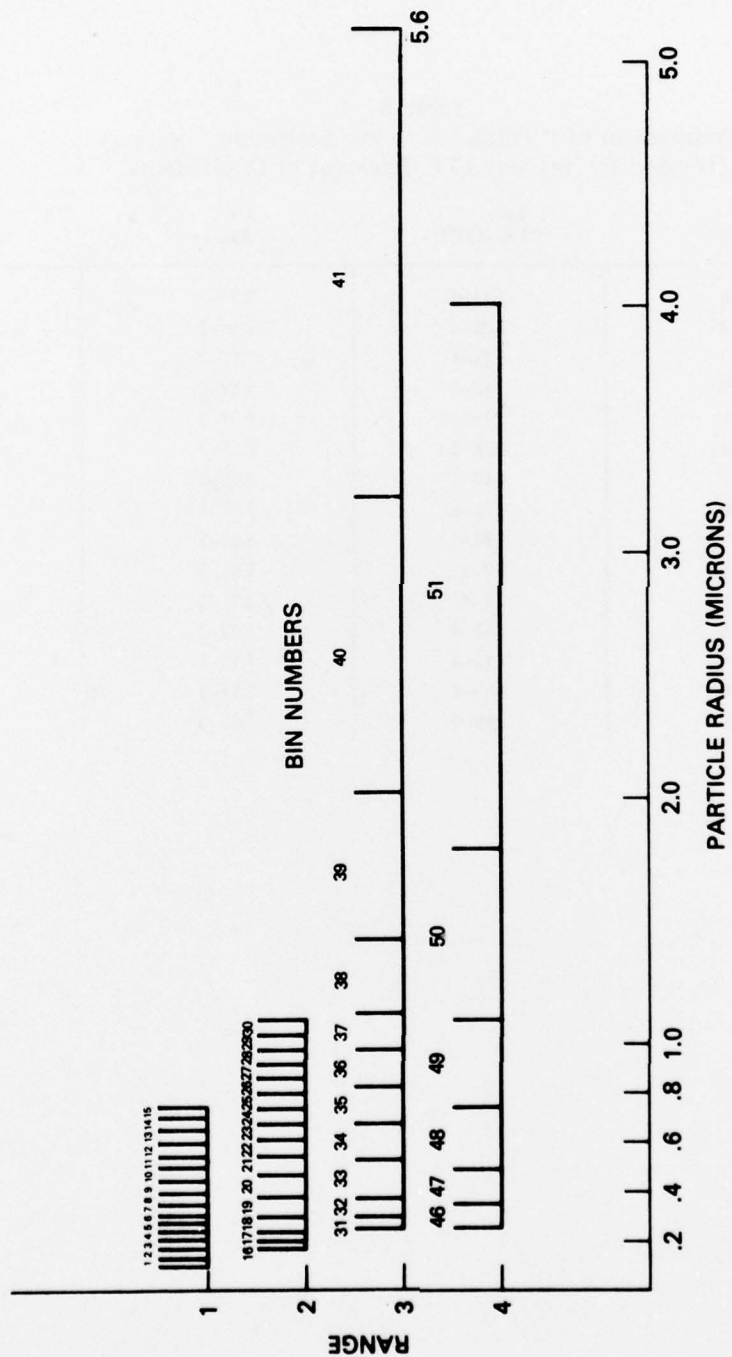


Fig. 1 — Particle size ranges for the Knollenberg counter

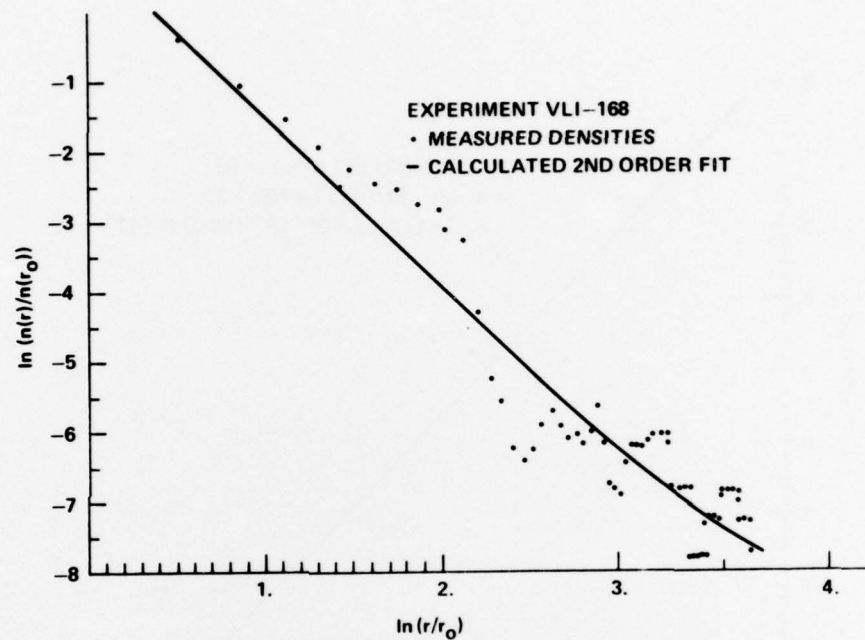


Fig. 2 — Particle size distribution versus radius.
Experiment VL1-168

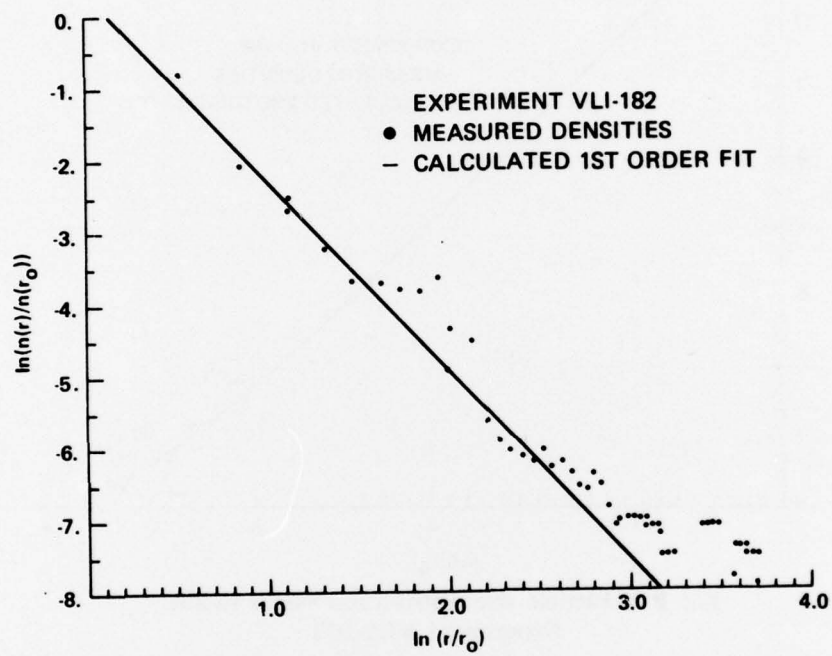


Fig. 3 — Particle size distribution versus radius
Experiment VL1-182

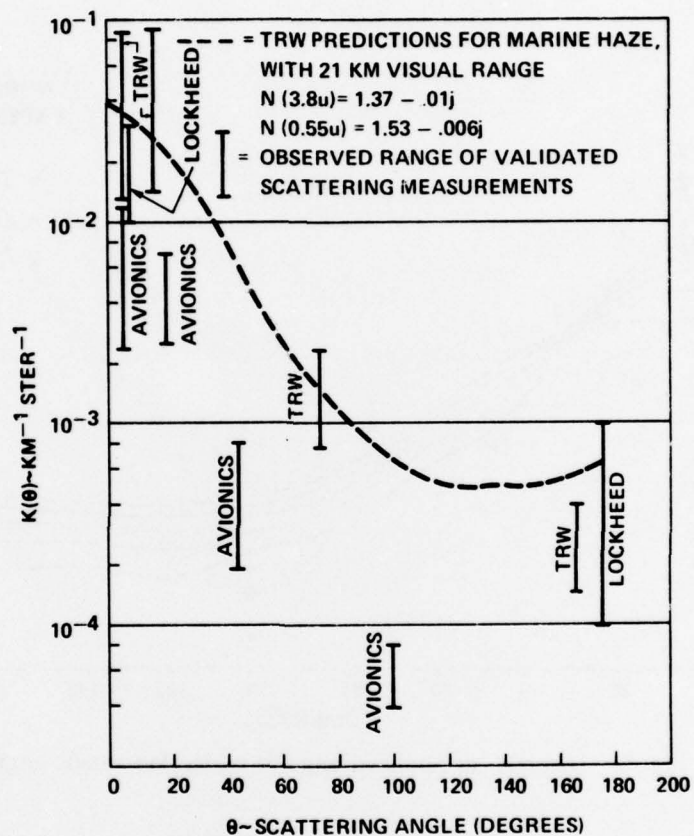


Fig. 4 — Data range for each experimental group at various angles

BEST AVAILABLE COPY

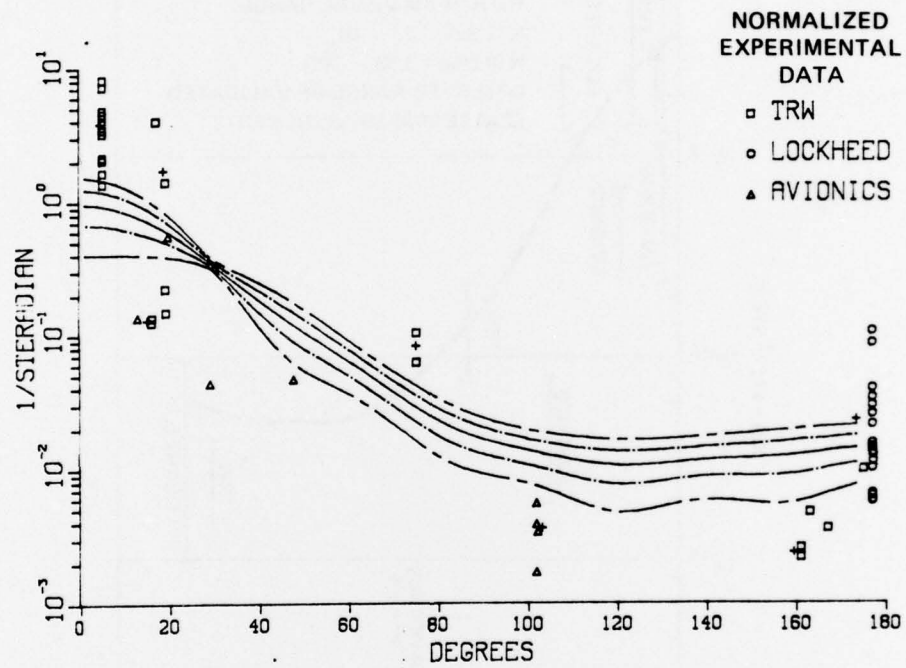


Fig. 5 — Average normalized angular scattering versus angle

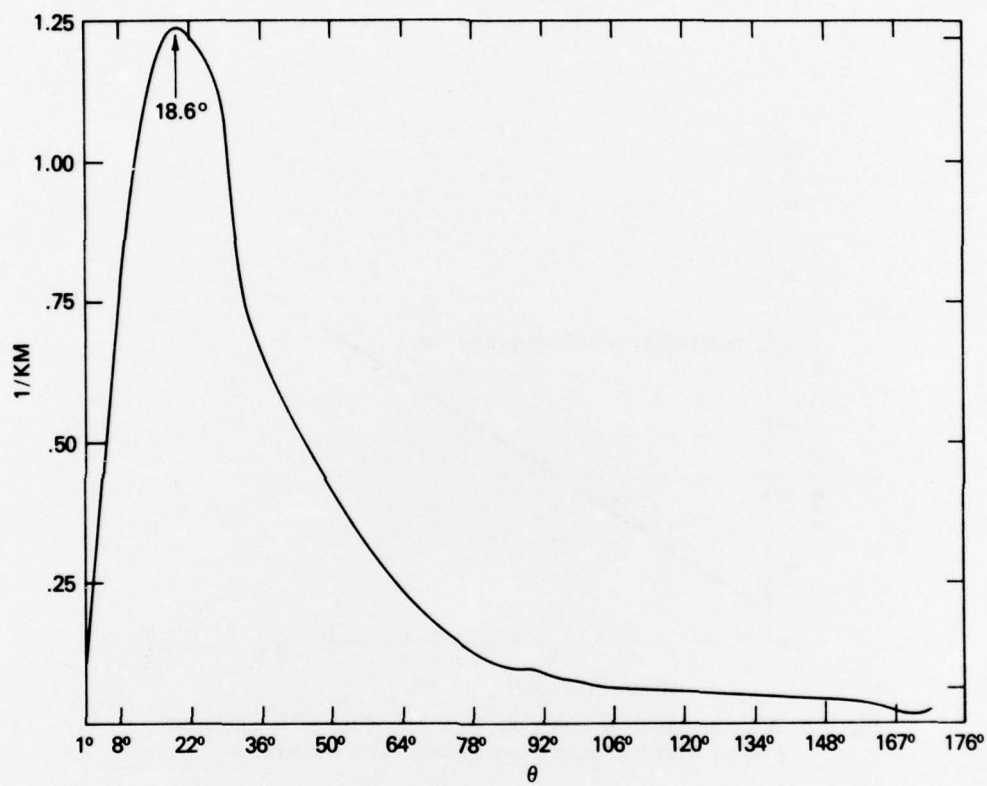


Fig. 6 — Average total scattering versus angle

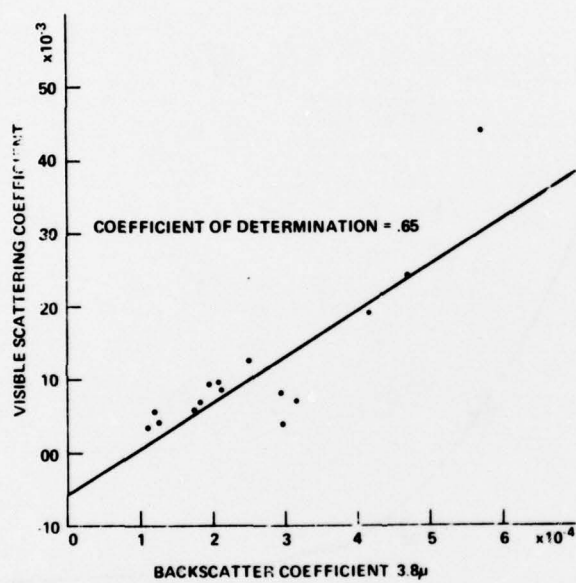


Fig. 7 — A Comparison of visible volume scattering coefficients/ 4π ($.65 \mu$) with backscatter coefficients at 3.8 microns